Chapter 10

Superposed Folds

In zones of orogenic activity it is common to find that rocks have been subjected to more than one phase of folding. The stresses which cause folding apparently wax and wane spasmodically, and frequently they also change in orientation too. In a major orogenic belt, such as the Appalachians or the Caledonides, in which a pronounced structural grain extends for several hundred kilometers, the fold axial trend is homogeneous only when the attributes of very large geographic areas are considered. When smaller objects (geographic areas) are studied, the increased detail reveals a more complex kinematic picture. In many orogenic belts, stress operated about different axes, and with different intensities, at different points in the space-time continuum.

As deformation proceeds the physical-chemical nature of the rocks slowly changes. In consequence, at successive phases slip, flexural-slip, or flexure folding may dominate within a particular domain; different types of deformation do not necessarily succeed each other in any particular sequence. At a given "instant" of geologic time one domain may be dominated by one type of folding, another domain by a different type that may even be folded about a differently-oriented *B*-axis. The spatial distribution of type and style of folding can be similar or different in a succeeding "instant." Commonly, when successive tectonic events affect an area, superposed folding results; it is very common, and may develop in any tectonically-active region, and in innumerable dissimilar tectonic and metamorphic environments.

Superposed folds have been recognized for more than a century. Scrope (1862, p. 291) referred to the phenomenon and cited examples from many parts of the world. Clough (in Gunn, *et al.*, 1897) and Peach *et al.* (1907, p. 601) showed that more than one direction of linear structures (including fold axes) had been recognized in several parts of Scotland. Although records of similar structures were slow to appear

in print, superposed folds must have been noticed in the field. For example, Van Hise and Leith (1911, p. 123) described superposed folding in the Soudan Formation, Vermilion Iron district, Minnesota, U.S.A.:

> The cross folding of the district has been only less severe than the major folding. . . . Both the longitudinal and the cross folds are composite—that is, folds of the second order are superposed upon the major folds in each direction, and upon these folds are folds of the third order, and so on down to minute plications.

In 1913 Crampton (in Peach, Horne, Hinxman, *et al.*, 1913, p. 57) described a "double system of folding" (a term borrowed from Peach, *et al.*, 1907) in central Ross-shire, Scotland. At about the same time Martin (1916, pp. 96 ff.) described "tranverse folds" in the Adirondack Mountains, New York, U.S.A. Tectonists such as Argand (1912, 1915) were also describing crossing fold trends in the European Alps, and Kober (1923) and Staub (1924) showed that interest in superposed folds continued there.

During the past decade the number of references to multiple folding has increased rapidly and some very thorough studies have been published (see Chapter 11). Nevertheless, despite this growth of interest, the number of published quantitative geometric syntheses of actual areas is quite small. Many accounts are partially subjective because sufficiently-detailed quantitative, objective, and appropriate structural data are lacking; in such cases it is almost impossible to evaluate the geometry objectively, or to be sure whether the correct interpretation has been made.

In Chapter 6 it was demonstrated that, even with very simple folds, the kinematic picture can be deduced only after complete analysis of the geometry. It is even more true that the complex kinematic pictures associated with superposed folds can only be tentative until the geometry is wholly elucidated. This involves careful definition of the populations of objects and attributes involved, and the use of clear operational definitions in the identification and measurement of each attribute.

CLASSIFICATION

First it is desirable to identify some of the variables involved in the development of superposed folds.

Superposition implies tectonic events distributed in time, but the intervals between successive events may range from infinitesimally short (geologically) to several hundred millions of years. Within a single orogenic episode, folding may have been limited to one or two pulses, or have been effected by numerous phases. Careful geometric analysis can commonly enable each phase of folding to be recognized, and each phase to be located on an ordinal time scale. Geometric analysis alone cannot determine the magnitude of the time-interval between successive phases of folding. Sometimes radiometric, paleontologic, or stratigraphic techniques may add precision, but commonly the intervals between phases of superposed folding are shorter than the error factors inherent in these techniques.

Second, the kinematic nature of the folds can vary. Three categories were established for simple folds in Chapter 6: (a) flexure folds, (b) flexural-slip folds, and (c) slip folds, although the boundaries between these groups are not sharp. In superposed folds the initial flexures may have been any one, or a combination, of these three types; similarly, the second and any subsequent phases can result from deformation of any type. Since the rheidity and the metamorphic milieu (including the possibility of diagenetic neocrystallization) almost certainly change with time, different types of folding commonly occur in the same suite of rocks during the successive deformation phases.

Third, the orientation of the stress field, and thus of the resultant strain pattern, can change. Such a change may be slight or very considerable, and it is described in terms of the angle between the B-geometric axes and/or the axial surfaces of the fold systems. Commonly a single B-geometric axis is not sufficient to define a superposed fold set (as will be described below).

These complex variables demonstrate that the development of superposed folds is not governed by a single universal principle. Although this may appear obvious, it is contrary to the views of some geologists. For example, Rast and Platt (1957, p. 159) complained that "cross-fold" has not been adequately defined, and implied that the term should be reserved for a narrowly-defined and genetically-related group of structures. Again, Lindström (1957, pp. 7 ff.) implied that structural geologists subscribe to one or another of the several "schools of thought," each of which advocates dissimilar unique principles about superposed folding. Although the concept of "schools of thought" may have some reality in this field of endeavor, as in that of, say, granite petrogenesis, the implication is unfortunate. Several of the authors referred to by Lindström have recognized the diversity of superposed folds and thus they do not fit into his supposed "schools."

THE CLASSIFICATION OF SANDER (1948)

Sander (1948) erected two groups of superposed folds:

(a) $B_1 \perp B_2$: the penecontemporaneous development of folds with axes perpendicular to each other; and

(b) $B_1 \wedge B_2$: the development of unrelated superposed folds by rotation about axes (B_1 and B_2) that are at any inclination to each other (including perpendicular).

In both cases triclinic fabrics result, although, considered separately, the deformation with respect to both B_1 and B_2 is commonly monoclinic.

The differentiation of these categories of Sander is more easy when the time dimension is emphasized. Although "penecontemporaneous" and "synchronous" are employed commonly in discussing $B_1 \perp B_2$-structures, the terms can be somewhat misleading. Sander pointed out that, in $B_1 \perp B_2$-folding, the two deformations are not precisely simultaneous throughout; that is, when small units of time are considered, the strain with respect to B_1 and B_2 (considered separately) is not strictly contemporaneous or continuing, but is spasmodic. Occasionally these spasms with respect to B_1 and B_2 may overlap in time, but Sander did not visualize a triclinic movement picture developed in a single act during an "instant" of geologic time. Anderson (1948, pp. 120 ff.) correctly pointed out that simultaneous slip in two perpendicular directions can be resolved into a single monoclinic movement picture; such a kinematic (movement) picture is contrary to Sander's hypothesis, because it assumes that the total movement was homogeneous with respect to time.

A hypothetical example may be considered. Prior to $B_1 \perp B_2$-folding suppose that the S-surfaces or planes (bedding, for example) are planar. If flexural-slip folding occurs at the commencement of deformation, monoclinic folds about B_1 are likely to be produced. These initial flexures may be of any size, from a small ripple lineation to open folds several tens of meters in amplitude. At a slightly later time (although synchronous with respect to development of the total structure) compression, normal to that which caused the folding about B_1, may cause rotation about B_2, a geometric axis normal to B_1. Although, with this type of flexural-slip folding, B_2 will always be normal to B_1, the B_2-axes must have varying orientations within the plane normal to the compression responsible for B_2. The dip and strike of S vary from point to point after the initial flexure about B_1, and the orientation of B_2 within this plane depends on the local dip of S (Fig. 281).

The style, size, and amplitude of the flexures developed about B_1 and B_2 may be similar, but commonly they are dissimilar. With this model,

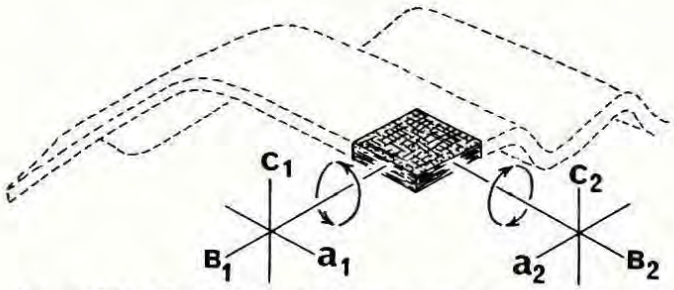

Figure 281. Resolution of triclinic strain into two mutually perpendicular monoclinic strains ($B_1 \perp B_2$) (After Weiss, 1959A, Fig. 13).

provided that a sufficiently small volume of rock is considered, both B_1 and B_2 are axes of monoclinic folding, although, in a larger volume of rock, the total deformation is manifestly triclinic. In a very small piece

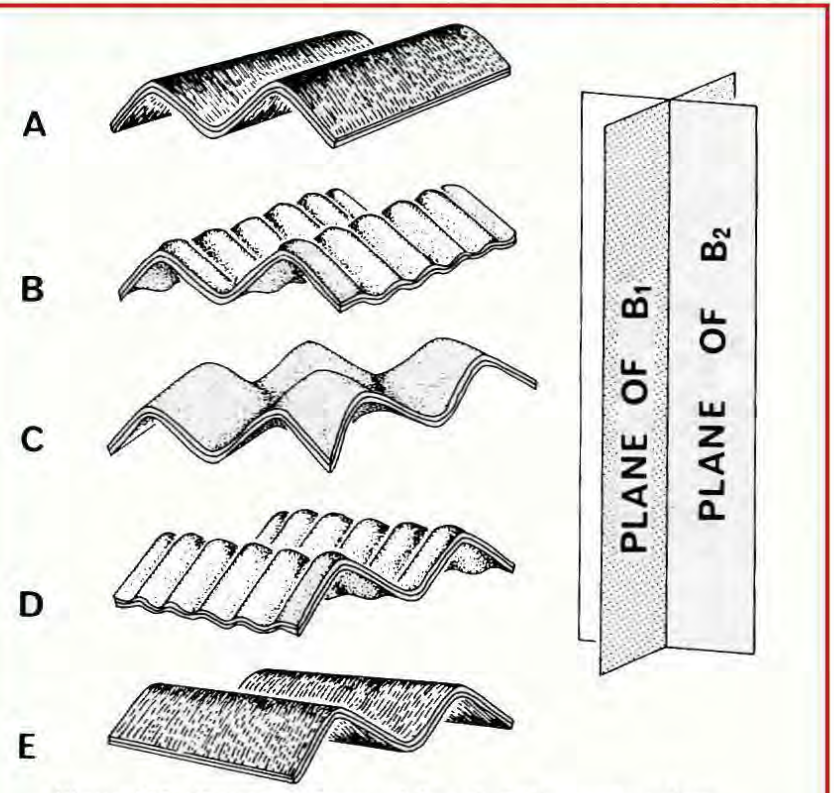

Figure 282. Geometric forms of $B_1 \perp B_2$-fold systems (After Weiss, 1959A, Fig. 12).

of rock within which S is still planar, B_1 is perpendicular to B_2 and both axes lie in S; hence, in a population of objects of this small size, $B_1 = a_2$, $a_1 = B_2$, and $c_1 = c_2$, as shown in Figure 281. When larger objects are considered, the plunges of both B_1 and B_2 vary; the variously-plunging B_1-geometric axes lie in a plane perpendicular to the plane containing the variably-plunging B_2-geometric axes. The mutual relationships of of B_1 and B_2 involved in $B_1 \perp B_2$-folding are illustrated in Figure 282. From the geometric point of view, the assigment of B_1 and B_2 to the two sets of axes becomes arbitrary, although, in the description of actual examples, it is common practice to designate the dominant set of folds as B_1.

To establish $B_1 \perp B_2$ it is necessary that folding about B_1 and B_2 was essentially synchronous on a regional-geographic and time scale. Weiss (1959A, p. 30) suggested that folds about B_1 and B_2 can continue to form synchronously once their general form has been established. In terms of large time units this may be possible, but with respect to small time units it is difficult to visualize how this could happen, or how it could be established with certainty.

With $B_1 \wedge B_2$ the unrelated superposed folds parallel to B_1 and B_2 are discretely separable in time, that is, folding about B_1 is completed before the B_2-folding is initiated; occasionally renewed, or posthumous, movement on B_1 can occur on a minor scale during subsequent deformation. Characteristically $B_1 \wedge B_2$-folding leads to very complex geometrical relationships.

Although reference has only been made to flexural-slip folds, neither $B_1 \perp B_2$ nor $B_1 \wedge B_2$ is restricted to a specific type of folding about B_1 or B_2.

THE PROPOSED CLASSIFICATION

Whitten (1959A) published a review of the described examples of superposed folds and developed a tentative, but unsatisfactory, classification. Sutton (1960A, pp. 153-54, 161) reviewed the superposed folds in the Scottish Highlands and drew up a complex and confusing pair of classifications.

It seems preferable to use a simpler scheme of classification, as follows:

A. $B_1 \perp B_2$-folds
B. $B_1 \wedge B_2$-folds
   1. B_1 and B_2 oblique but penecontemporaneously developed
   2. B_1 and B_2 superposed but developed during the same general orogenic phase

3. B_1 and B_2 superposed and developed during long-separated cycles of orogeny.

In each case the $B_1 \wedge B_2$-folds can be further subdivided according to whether:

(a) the preferred orientations of B_1 and B_2 are parallel, oblique, or perpendicular to each other, and

(b) folds about B_1 and B_2 are of flexural-slip, slip, or flexural type, or some combination of these types.

Many natural occurrences are, of course, transitional between these artificially-erected categories.

The interrelationship of these variables is shown in Figure 283. This three-dimensional classification system suffices when only two phases of folding were superposed, but additional dimensions are required to incorporate multiple superposition (i.e., three or more fold phases). For example, a third phase of folding requires a five-dimensional system; the fourth dimension would be divided into the same categories used for the second folding in Figure 283, and the fifth dimension would be divided

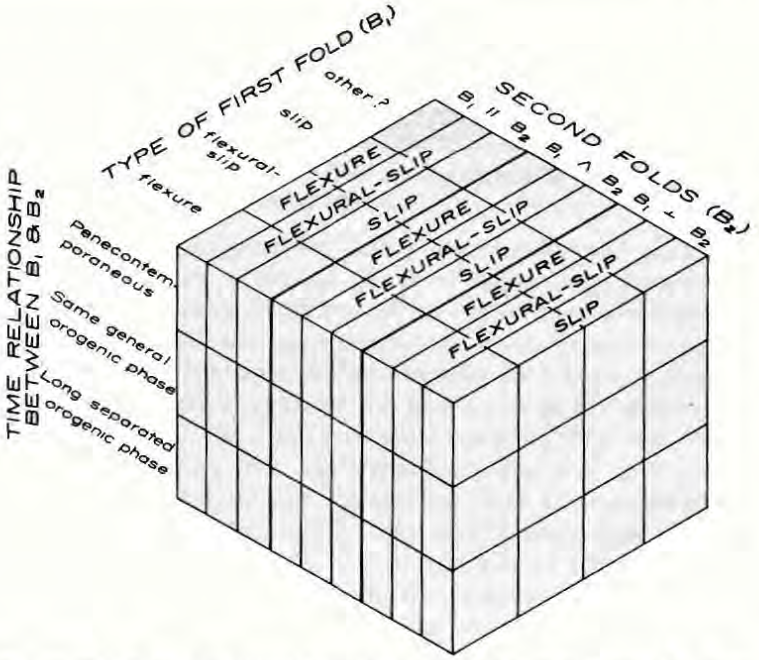

Figure 283. Possible interrelationships between two superposed phases of folding where each phase may be flexure, flexural-slip, or slip folding.

on the basis of the time relationships between the third and the earlier phases of folding.

Strong arguments for a genetic classification of superposed folds could be advanced. Apart from the general physical conditions during the folding (e.g., rheidity and the metamorphic milieu), the nature of the changing stress field would then be of paramount importance. Although a genetic classification might be an eventual aim, it is so difficult to determine the stress field for a folded sequence of rocks that, even when the strain picture is reasonably well known, it is impractical and dangerous to assay a genetic classification at the present time.

A variety of overlapping terms has been used recently for superposed folding. "Cross fold," "crossing fold," "transverse fold," "crossfold," "(cross-)fold," and "superimposed fold" have all been employed (see Whitten, 1959A). To avoid confusion with some of the earlier definitions (Nevin, 1949; Bhattacharji, 1958, 1959) "superposed fold" is used in this book (cf. Weiss, 1959B; Roach, 1960).

THE GEOMETRY OF SUPERPOSED FLEXURAL-SLIP FOLDS

The geometry involved when two sets of cylindroidal flexural-slip folds are superposed to produce $B_1 \wedge B_2$-folds is relatively simple. $B_1 \wedge B_2$-structures must be considered in three dimensions, and the most realistic current method is to use stereographic projection. The principles can be illustrated most easily with a hypothetical example.

In Figure 284 a single bed within an antiform is illustrated. It is assumed that the ground surface is horizontal. The fold axis plunges to 060 at 28° and the axial plane dips to 110 at 40°. In the east the beds dip to the east, while on the west flank the beds are overturned and dip southeast. These relationships are illustrated by stereographic projection in Figure 285. For simplicity the limbs of the fold are broken into short planar sections, each of which is plotted on the stereogram, which is a composite π- and β-diagram (Fig. 285). The great circle containing all of the S-poles is shown and $B_1 = \beta$.

Now assume that a small ripple-like linear structure parallel to B_1 is visible in most exposures of the map area (Fig. 284); alternatively, it may be assumed that numerous small parasitic folds are homoaxial with the main structure. It will be assumed that these minor structures can be identified after superposed folding.

It is reasonable to assume that the first deformation was caused by compression approximately normal to the axial plane. Suppose that a

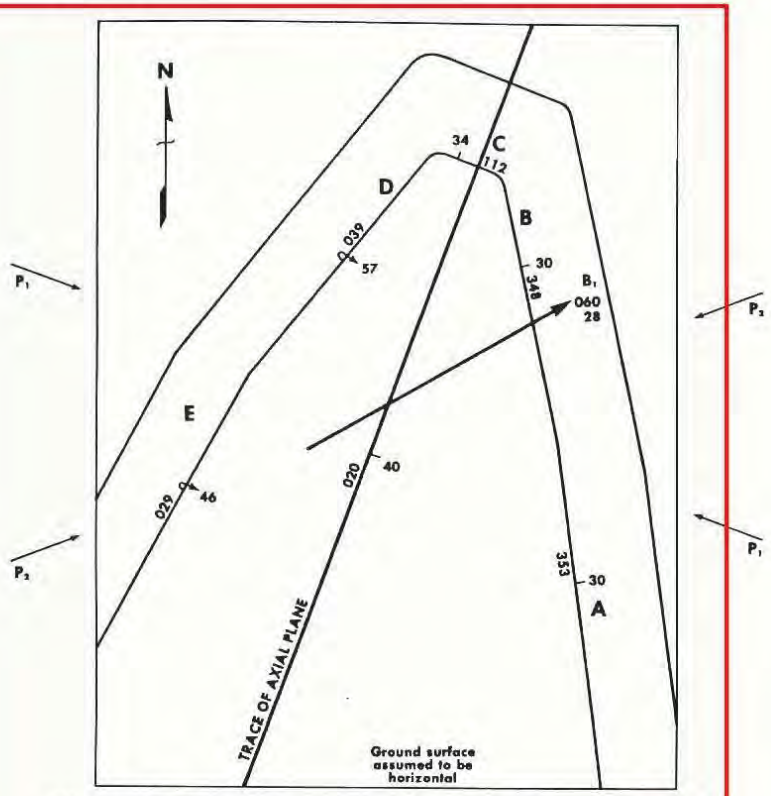

Figure 284. Schematic map of a plunging anticline with ground surface assumed to be horizontal.

second phase of compression acting horizontally and parallel to P_2 (Fig. 284) produces a second phase of flexural-slip folding so that $B_1 \wedge B_2$-folding results. Each bed of the earlier structure folds about a new axis (B_2) lying in the plane normal to the new compression axis, P_2. A separate second fold axis, B_2, develops for each bedding plane with a different dip and strike. Because the B_2-axes lie in the plane normal to the compression P_2, they plot on a great circle (cf. Braitsch, 1957).

A single *S*-surface from the original anticline (Fig. 284) can be used for illustration. In Figure 286 the bedding plane C (from the closure of the fold) is used; this bed had a strike of 112 and it dips north at 34°. The great circle normal to P_2 is a straight line in Figure 286, and the bedding plane C intersects it at B_2, the second fold axis with *respect to this particular S-surface (C)*. As the second phase of folding continues, the *S*-surface C rotates about B_2; this can be illustrated by a π-diagram or a β-diagram. The *S*-pole (π_{C_1}) for C rotates about B_2 during the second folding, and successive positions of π_{C_1} (designated π_{C_2},

Overall geometry of First phase before refolding

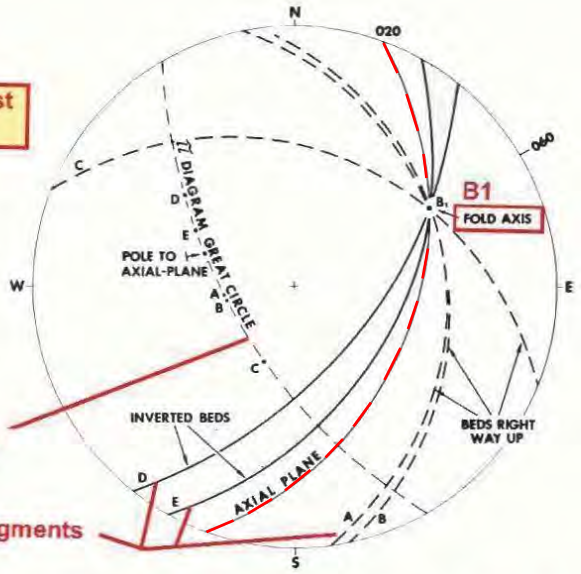

Figure 285. The geometry of the fold in Figure 284 shown in stereographic projection. The points A through D represent π-poles of the bedding planes indicated by the great circles (A through D) that intersect in B_1.

great circle of poles to fold segments

Bedding in fold segments

Geometry of segment (C) after refolding

rotation of B1 and L1 along small circle due to refolding

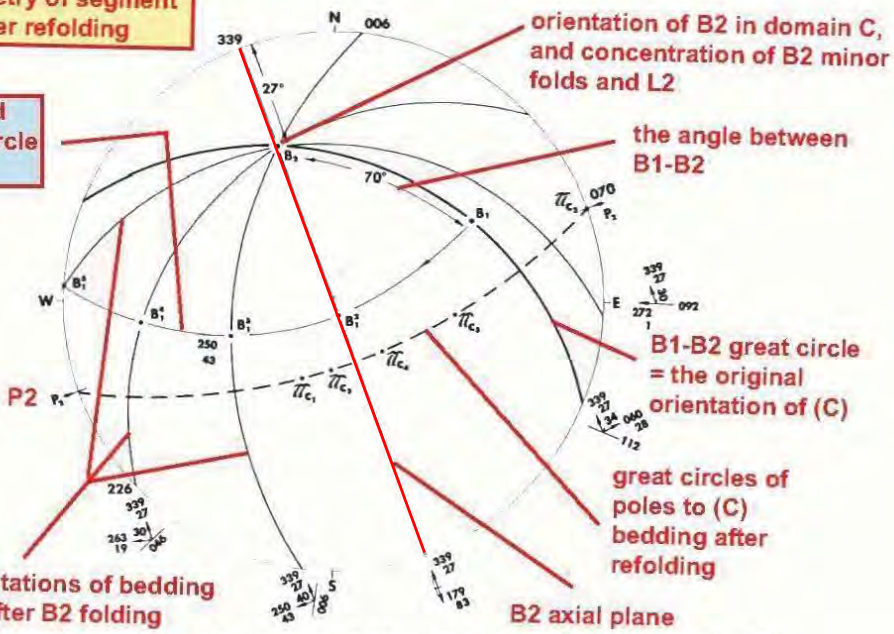

Figure 286. Superposed flexural-slip folding (B_2) of bedding plane C (from Fig. 284) as a result of compression about P_2. The great circle through B_1 and B_2 is the original bed C; the other great circles through B_2 are possible orientations of C after B_2-folding; poles to these rotated bedding planes (π_{C_1}, π_{C_2}, ...) lie on the great circle (broken line) through P_2. Early lineations parallel to B_1 (B_1^2, B_1^3, ...) lie on the small circle about B_2. Map symbols appropriate to the rotated C-planes are shown outside the margin of the projection.

$\pi_{C_3}, \ldots, \pi_{C_n}$ in Fig. 286) lie on a great circle because the angular distance between B_2 and π_{C_1} is 90°.

The linear structures parallel to B_1 (B_1 in Fig. 286) rotate with S during the second deformation. However, B_1 moves along a small circle because the angular distance between B_2 and B_1 is not 90°; the angle happens to be 70° in Figure 286. B_1 assumes positions B_1^2, B_1^3, B_1^4, . . ., B_1^n as π_{C_1} rotates to $\pi_{C_2}, \pi_{C_3}, \pi_{C_4}, \ldots, \pi_{C_n}$ (Fig. 286).

The field observations which would be associated with the successive positions of C are shown at the bottom of Figure 286. While the second linear structure (B_2) maintains a *constant* orientation, the first linear element has a very *variable* orientation ($B_1^2, B_1^3, \ldots, B_1^n$).

As another example, bed E, from the inverted limb of the anticline (Fig. 284) is shown in Figure 287; the strike is 029 and the dip 46° east. Figure 287 is primarily a β-diagram resulting from rotation of the S_0-surface (E) about the second fold axis B_{2_E}. The poles to the rotated S_0 are $\pi_{E_2}, \pi_{E_3}, \ldots$, and the great circle containing them passes through P_2 (cf. Fig. 286). The second folding causes the linear elements B_1 (B_1 in Fig. 287) to move along a small circle to successive positions $B_1^2, B_1^3, \ldots B_1^n$; B_1 and B_1^2 are on inverted limbs, whereas B_1^3, B_1^4, B_1^5, and B_1^6 are on S_0-surfaces that have returned from inverted positions to the correct way up. At the bottom of Fig. 287 field observations appropriate to several of the S_0-surface orientations are shown.

It is commonly helpful to compile synopses of the relationships exhibited by all the elements of the structure within an area. Figure 288 is a **synoptic diagram** based on operations like those used for Figures 286 and 287. Compression P_2 induced a second generation of folds with respect to each of the five planar sections (A, B, C, D, and E) of the original S_0-surface (Fig. 284). For each planar section a new fold axis has been developed that lies in the new axial plane normal to P_2. The five new fold axes are B_{2_A}, B_{2_B}, B_{2_C}, B_{2_D}, and B_{2_E} in Figure 288. It is a general property that each of the great circles defined by the poles to the refolded S_0-surfaces intersect in P_2. A further general property is that small circles drawn through the projections of rotated first linear elements (B_1) intersect at B_1 (Fig. 288); this is intuitively reasonable, because, for each position of S_0 the linear elements initially coincide with B_1, and during the second deformation they are progressively rotated from this direction. These relationships of the small and great circles on synoptic diagrams are useful in analyzing the geometry of an area.

For each generation of folds, the amplitude, style, and size of the flexures, and also the nature of the linear structures, are commonly

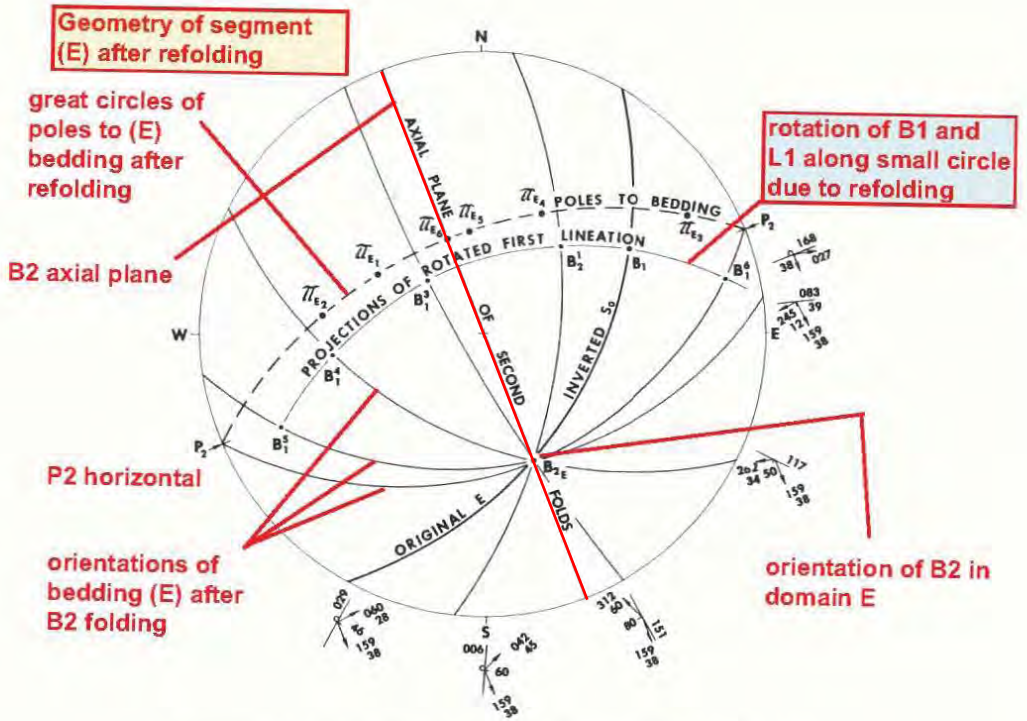

Figure 287. Superposed flexural-slip folding (B_2) of inverted bed E (from Fig. 284) as a result of compression about P_2. The explanation is the same as for Figure 286.

Synoptic Diagram

Figure 288. Synoptic diagram representing flexural-slip folds produced by compression P_2 affecting the fold B_1 of Figure 284. The great circles (light lines) intersecting in P_2 are defined by poles to the rotated S_0-planes. The small circles (heavy lines) intersecting in B_1 are defined by the rotated first fold linear elements that were parallel to B_1.

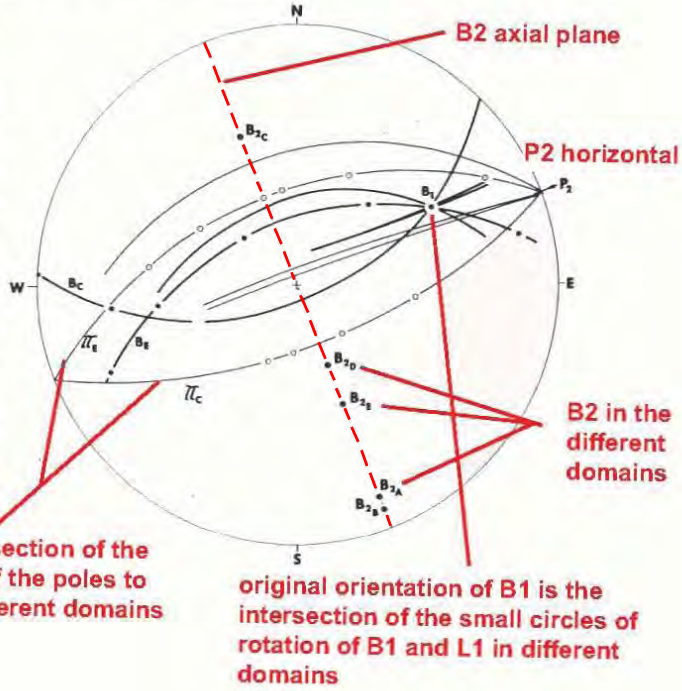

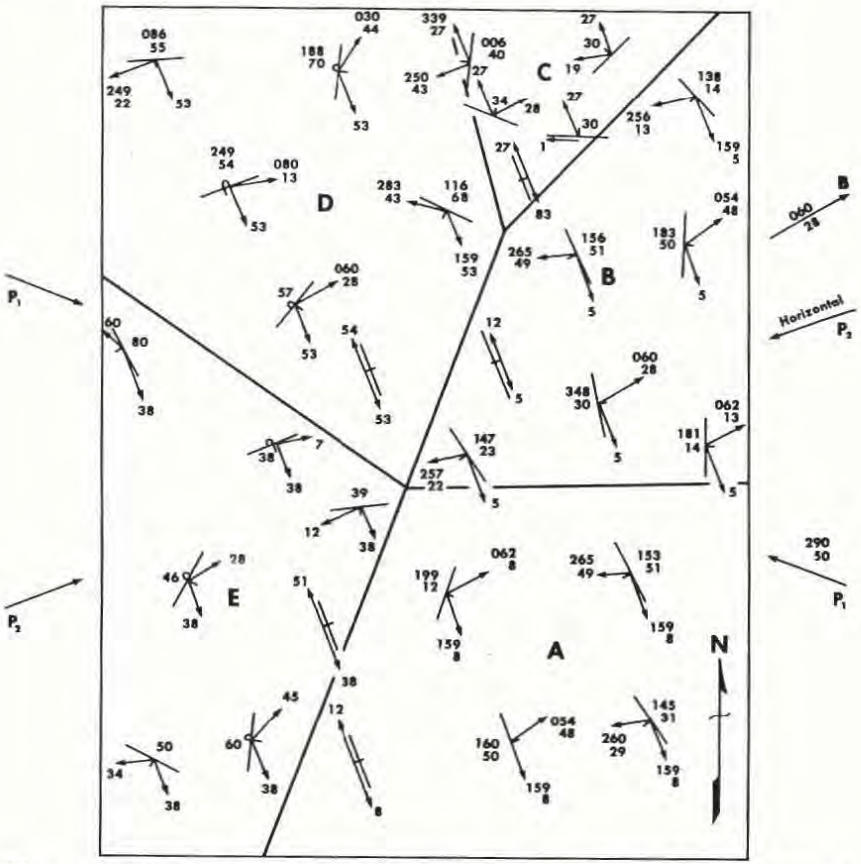

Figure 289. Schematic map of an area (Fig. 284) in which $B_1 \wedge B_2$-flexural-slip folding has occurred (the ground surface is assumed to be horizontal).

distinctive. Such differences can be very significant in analyzing superposed folds. Thus, the importance of observing and recording the distinctive characters of fold structures in the field cannot be overemphasized.

Even in those cases in which the fold and linear structures produced during both phases of $B_1 \wedge B_2$-folding are similar, the geometric relationships should enable the fold geometry and the sequence of events to be unravelled. The technique can be illustrated with the aid of the map shown in Figure 289.

The map of an area in which superposed flexural-slip folding occurred (Fig. 289) can be divided into subareas within which the S-surfaces were approximately planar at the close of the first folding. Theory dictates that the second deformation results in a parallel set of linear

structures in each such subarea. For example, in the northwest part (area D) of Figure 289, one linear element plunges to 159 at 53° at each locality. Again, throughout the southern half of the map a linear structure trends at 159, but the plunge differs in each subarea (Fig. 289, areas A and E). Linear structures induced by the second deformation are constant in orientation in each domain. Linear structures of the first deformation now have variable orientations within each subarea.

In actual field studies, it is commonly quite difficult to delimit suitable geographic subareas. Current methods tend to be largely empirical, but one guide is to prepare a map of all the linear elements only. Geographic areas within which similar linear elements are approximately parallel (homogeneous) can then be isolated. Boundaries defined by this principle are marked on Figure 289.

If linear elements are not abundant, subareas can often be defined by locating domains within which S-poles lie close to a great circle on a π-diagram. This is strictly a trial-and-error process, and the boundaries of subareas are adjusted to include only S-poles that lie close to the great circle. Exposures at the domain boundaries can often be accommodated in either subarea.

domain choice

The great circle suitable for an array of points is found by rotating the tracing paper over the Wulff graticule; as the great circles of the graticule pass beneath the plotted points, the one of best fit is chosen by eye and traced on the plot. Finding a small circle is more difficult, unless its center happens to lie on the primitive circle, when a small circle printed on the Wulff graticule can be traced onto the plot. A method appropriate for all other cases is illustrated in Figure 290 (which is based on the β-diagram of Fig. 287). Suppose the dots are projections of linear elements and that it is required to know whether they lie on a small circle about B_{2_E}. The angular distance from B_{2_E} to one of the clusters of points is measured along a great circle. This angle is then measured off from B_{2_E}, along several other great circles passing through B_{2_E}, to give the points a, b, c, d, ... The smooth curve passing through a, b, c, d, . . ., is the required small circle. Since the circle passes through the second cluster of linear elements, both groups of projections lie on the same small circle. An additional small circle 20° from B_{2_E} has been plotted on Figure 290 by using the same method.

In the hypothetical example (Fig. 289), the structural elements from each subarea can be plotted on separate stereograms; for example, Figures 286 and 287 represent subareas C and E, respectively. When transferred to a synoptic diagram the small circles intersect at the location of the first linear element, B_1 (cf. Fig. 288); the intersection of the great circles defines the orientation of the second compression (P_2).

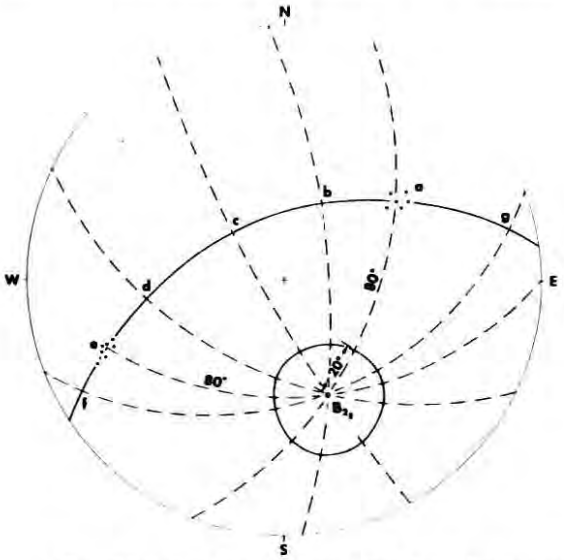

Figure 290. Construction of small circles about B_2 on a stereographic projection. For explanation see text.

Complication stems from the fact that commonly the second maximum compression axis (P_2) is not necessarily horizontal. When P_2 has a marked plunge, the trends of the second linear elements are no longer constant over the map area. However, the trend is constant within each subarea in which S_0 was planar at the close of the first deformation (e.g., within subareas A, B, C, D, and E of Fig. 284). The geometry can be illustrated by using the structure of Figure 284, but allowing P_2 to plunge at, say, 60° to the northeast. Figures 291 and 292 portray the resulting geometry of subareas C and E, respectively; these diagrams correspond to Figures 286 and 287. Figures 291 and 292 show that the trends of the second fold axes B_{2_C} and B_{2_E} are not parallel (whereas they are parallel in Figs. 286 and 287). However, as when P_2 was horizontal, the present B_{2_C} and B_{2_E} lie on a great circle normal to P_2. Some representative positions of S_0 are drawn as a β-diagram in Figures 291 and 292, and they are also plotted on a map (Fig. 293) for comparison with Figure 289.

For these geometric analyses it is not necessary to have a detailed map of the lithologic units. Naturally, however, this information is required if a complete picture of the style of the folding is to be obtained and if the original stratigraphic succession is to be interpreted. However, even where the lithologic units have been carefully mapped, and sufficient structural data are available for the geometric style to be interpreted, it is difficult to predict the behavior of a lithologic unit outside the area of the immediate survey. For example, Knowles, *et al.*, (1962) mapped the metamorphosed Precambrian iron formation in the Julienne Lake area, Labrador, Canada, and deduced the geometric style of the superposed

Geometry of segment (C) after refolding. P2 is inclined

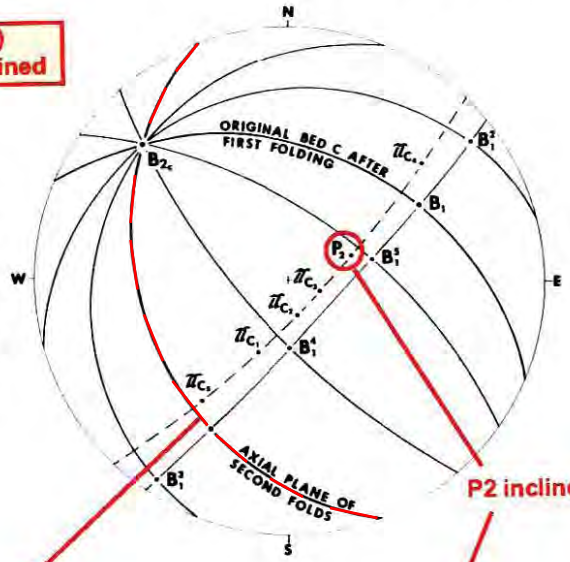

Figure 291. The geometry of subarea C (of Fig. 284) resulting from superposed flexural-slip folding due to compression P_2. The axial plane of the second folds is normal to P_2. The notation is as in Figure 286.

P2 inclined

B2 axial plane

Geometry of segment (E) after refolding. P2 is inclined

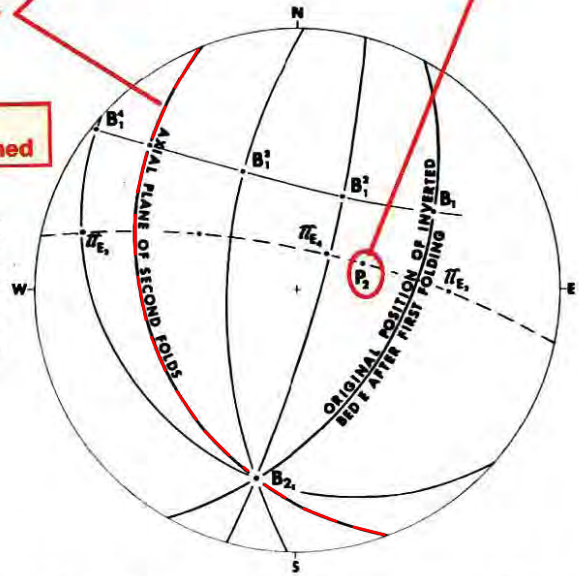

Figure 292. The geometry of subarea E (of Fig. 284) resulting from superposed flexural-slip folding due to compression P_2. The notation is as in Figure 286.

folding (Fig. 294). With the methods available at present, it is difficult to predict the precise location of such a doubly-folded ore body at depth or outside the limits of the immediate mapped area.

In the examples discussed above the original S_0 was assumed to be absolutely planar, and the two stress fields (responsible for B_1 and the

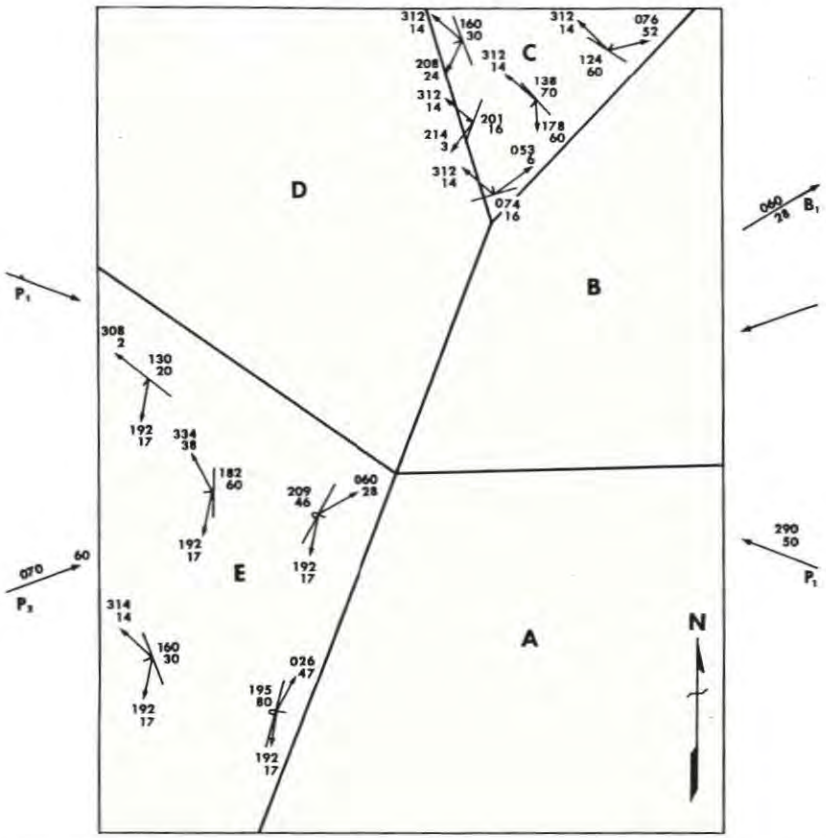

Figure 293. Schematic map of an area (Fig. 284) in which $B_1 \wedge B_2$-flexural-slip folding has occurred as a result of compression along an axis (P_2) plunging at 60°. See text for full explanation.

B_2-axes) were taken to be uniform throughout the map-areas. Thus, in Figure 289 the map has idealized geometry. In actual examples some variability occurs, and it cannot be anticipated that the field data will approximate too closely with great and small circles. However, by careful selection of the limits of subareas, domains that are approximately homogeneous with respect to specified attributes (such as a specified second lineation) can commonly be isolated. Even when small domains are carefully selected, a slight scattering of points is to be expected; that is, the areal distribution has subsystematic tendencies (see Chapter 3).

In all of these constructions it was assumed that the axial surfaces of the second generation folds are subparallel and planar. Undoubtedly this simplification does not always apply in natural examples, although

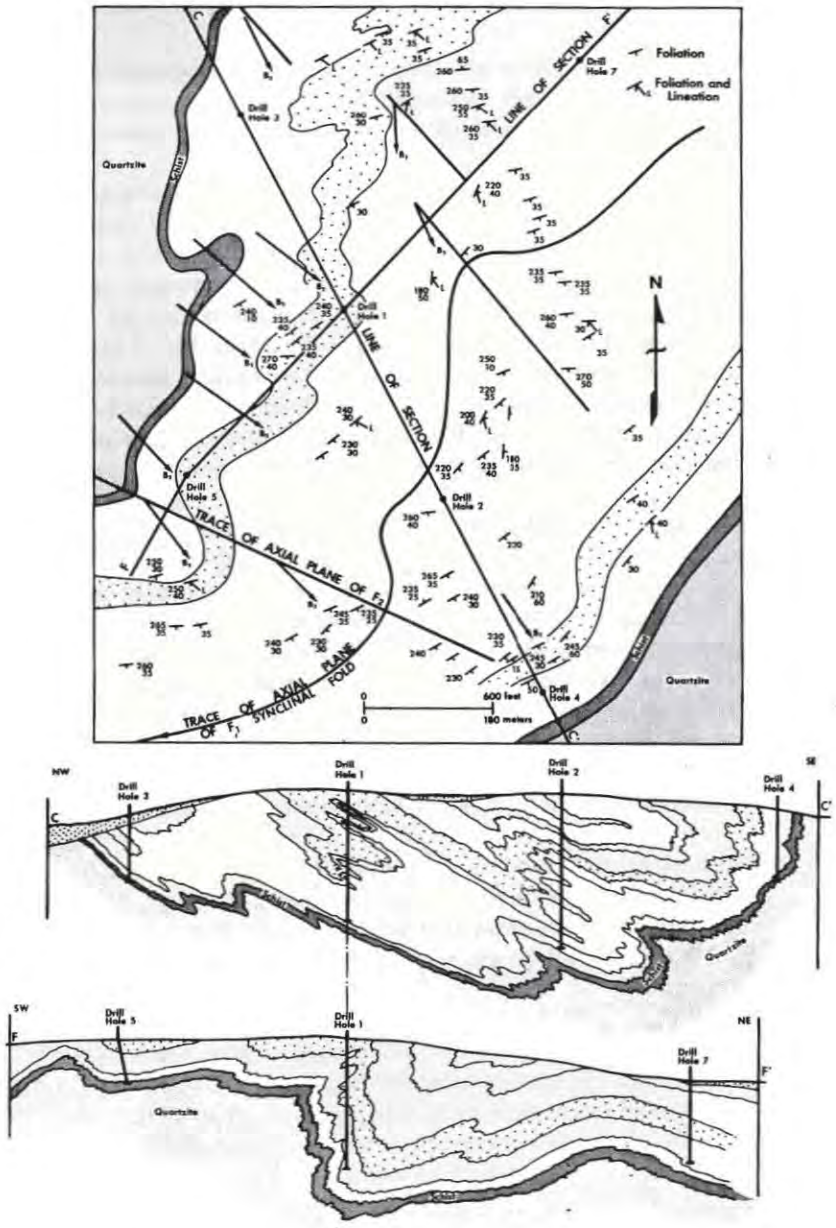

Figure 294. Superposed folds affecting the Precambrian iron formation in the Julienne Lake-Wabash Lake area, Labrador, Canada; the cross-sections show the fold styles as determined by mapping and drilling (Based on manuscript map dated 1960 and made available by Mr. D. M. Knowles).

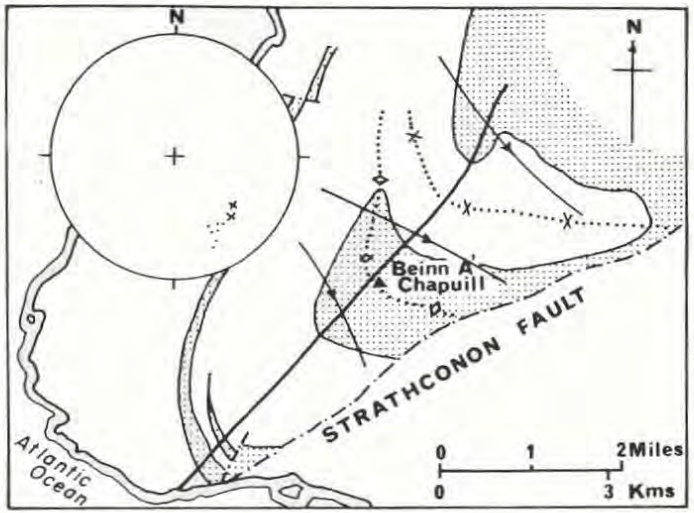

Figure 295. Map of folds in the Beinn a' Chapuill area, S of Glenelg, Northern Highlands, Scotland. Axes of both minor folds and of linear structures associated with the late folds plunge SE (represented by long arrows on map): note how they diverge from the antiform and converge on the synform. *Inset*: Late linear structures—dots are linear structures on NE limb of early synform and SW limb of early antiform; crosses are linear structures on the common limb of the two early folds (After Ramsay, in Clifford, *et al.*, 1957, Fig. 11).

as Weiss (1959B, p. 95) pointed out, such subparallelism has been described for several natural superposed fold systems. Sander (1948, pp. 177-78) referred to such features, and Weiss and McIntyre (1957, pp. 596-600) described examples from the Dalradian tectonites of Loch Leven, Scotland. Figure 295 shows the Beinn a' Chapuill region, south of Glenelg, W Scotland, in which Clifford, *et al.* (1957, p. 19) mapped a superposed set of folds with a constant axial plane orientation.

THE GEOMETRY OF SUPERPOSED SLIP FOLDS

In Chapter 6 the distinctive geometry of slip folds was described; a superposed second phase of deformation may be of this type. Slip folds

may be superposed on either flexural-slip or slip folds. Figure 296 is a diagrammatic sketch-map that illustrates the changes in geometry as progressively more penetrative slip folding is superposed on flexural-slip folds.

The effects of superposed slip folding can be illustrated by reference to the fold in Figure 284. The S-surfaces S_A, S_B, . . ., S_F resulting from the first folding are shown as a β-diagram in Figure 297. In this case $\beta_1 = B_1$. Superposed slip folding, resulting from slip on planes normal to P_2, will be considered; P_2 plunges with the same orientation as in Figure 293. In Figure 297, S' is the plane normal to P_2 and parallel to the new (second) axial-plane foliation. The kinematic axes during the second phase of folding can be designated a_2, B_2, and c_2; c_2 coincides with P_2, while a_2 and B_2 lie in S'. In Figure 297, a_2 and B_2 have been assigned arbitrary positions, but the location of a_2 controls the geometry of the second folding.

It follows from the discussion of slip folding in Chapter 6 that the second fold axis (β_2) lies at the intersection of S' and the original S, and that, in general, $\beta_2 \neq B_2$. Hence, the superposed folding produces a separate fold axis in each subarea. For example, in Figure 297, S_A yields the new fold axis β_{2_A}, S_B yields β_{2_B}, etc. As folding proceeds the S-surface in each domain is rotated about the new fold axis (β_2), and all first deformation linear elements parallel to B_1 rotate in the plane passing through B_1 and a_2. Thus, the projections of the rotated B_1-linear elements lie on the great circle containing B_1 and a_2; this is the same great circle for each domain. The geometry of this type of deformation was described by Weiss (1955, Fig. 1).

A few possible orientations of S_C following the second folding are shown in Figure 298; these were derived by rotation of rocks in subarea C (Fig. 284) about β_{2_C}. Possible rotated positions of B_1 are indicated by B_1, $B_1^?$, $B_1^?$, ... The corresponding geometry for subarea E (Fig. 284) is shown in Figure 299; each subarea yields a separate β-diagram, as shown synoptically in Figure 300. The results from Figures 298 and 299 are illustrated as a map in Figure 301.

In these diagrams none of the intersections of S and S' coincide with either of the kinematic axes a_2 or B_2. In a domain in which the intersection of S and S' is parallel to the a_2-kinematic axis, the S-surfaces are not folded because the slip is parallel to S (see Chapter 6). Should the intersection of S and S' be parallel to the B_2-kinematic axis, the second axis of folding (β_2) is parallel to B_2, and $B_2 = \beta_2$.

In the illustrations used above, the first folds were flexural-slip, so that $B_1 = \beta_1$. The geometry of the superposed folds would not be altered if

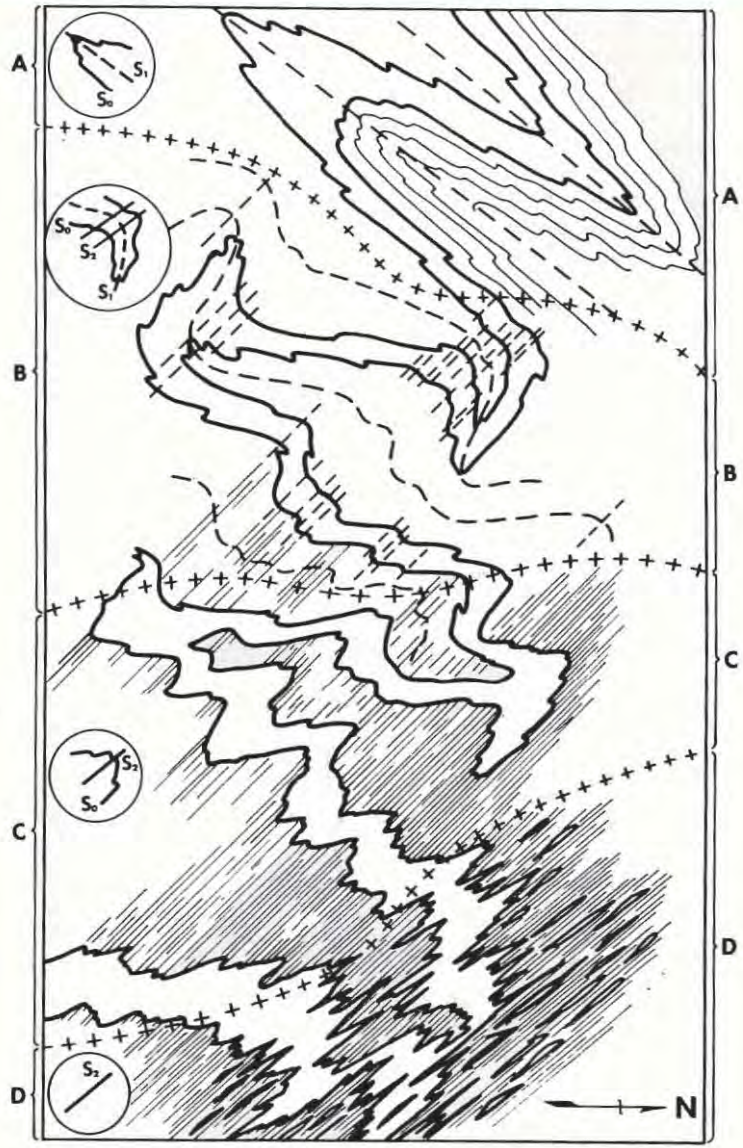

Figure 296. Hypothetical geological map showing transposition structures associated with superposed folds. Domains A through D show progressive stages of superposition of folds with axial planes striking NW; axial planes of the earlier folds strike NE. Transposition of the initial S-structure (S_0) into the secondary foliation S_2 is complete, on the scale of the map, in domain D (After Turner and Weiss, 1963, Fig. 5-26).

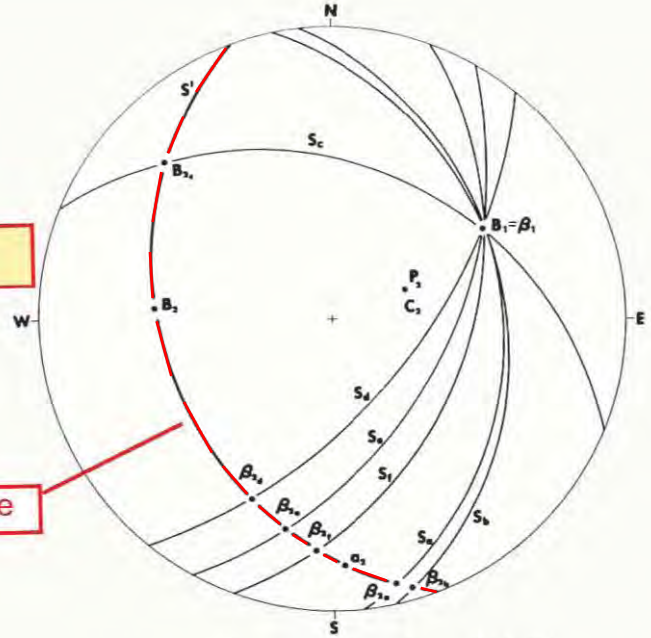

Figure 297. New fold axes resulting from slip folding superposed on the B_1-fold of Figure 284. The first fold is represented as a β-diagram; β_{2A}, β_{2B}, ... are the axes of second generation folds resulting from slip on S' normal to P_2. The orientation of the kinematic a_2- and B_2-axes within S' has been chosen arbitrarily.

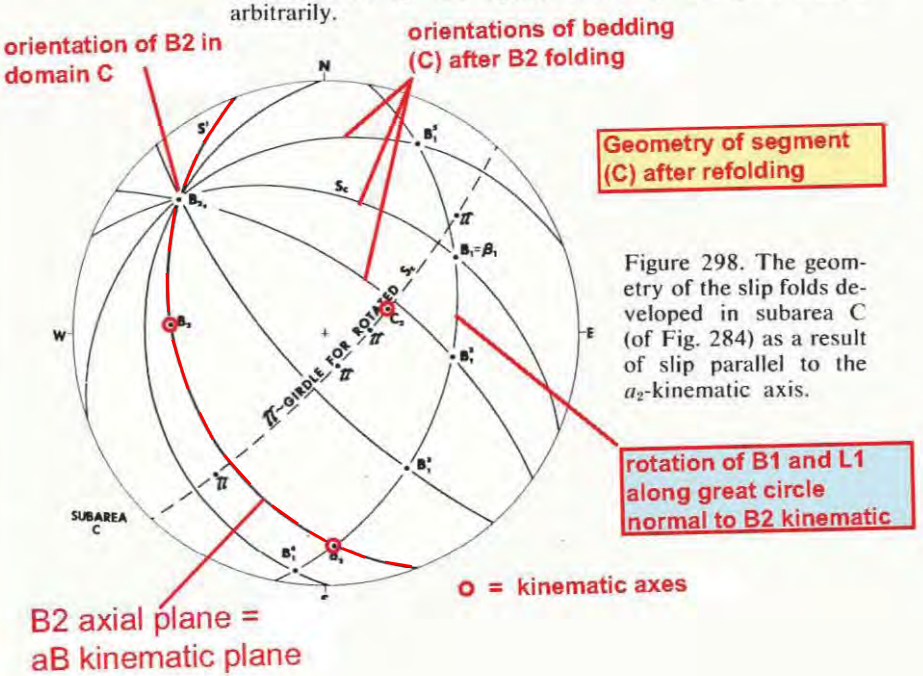

Figure 298. The geometry of the slip folds developed in subarea C (of Fig. 284) as a result of slip parallel to the a_2-kinematic axis.

2 axial plane =
B kinematic plane

orientations of bedding
(E) after B2 folding

Geometry of segment
(E) after refolding

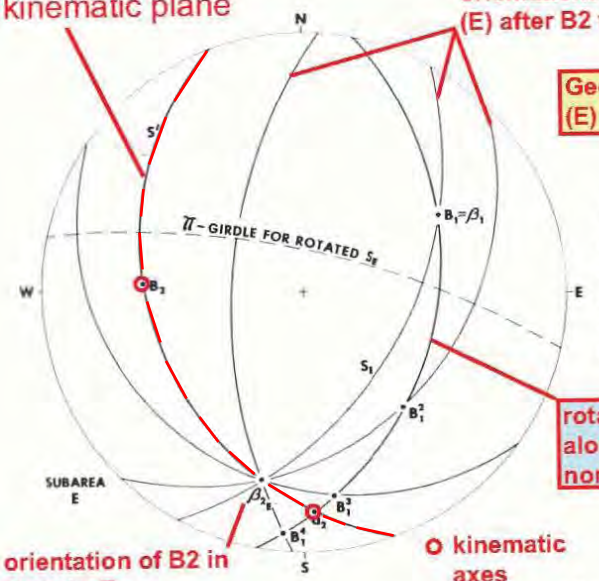

Figure 299. The geometry of slip folds in subarea E (of Fig. 284) produced by slip parallel to an a_2-kinematic axis normal to P_2.

rotation of B1 and L1
along great circle
normal to B2 kinematic

orientation of B2 in
domain E

O kinematic
axes

old lineations
axes of minor
folds (L1 & B1)
lie along great

Synoptic Diagram

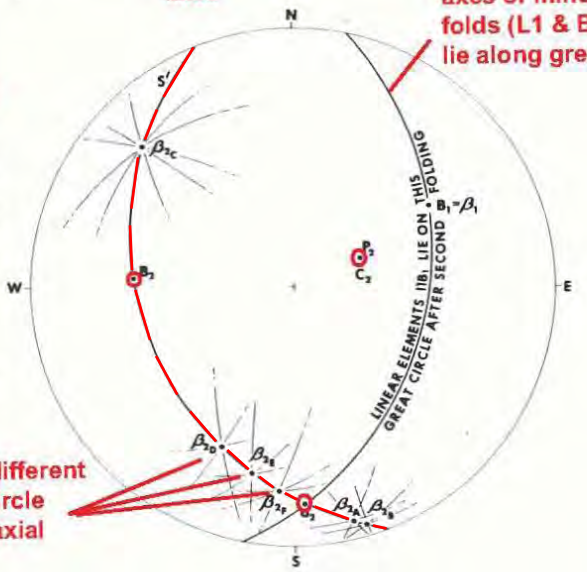

Figure 300. Synoptic diagram showing the geometry of slip folds throughout the area of Figure 284 that result from slip parallel to an a_2-kinematic axis normal to P_2. The great circles (light lines) passing through β_{2A}, β_{2B}, . . . represent the folded S-planes in each subarea.

the orientations of B2 in different
domains lie along great circle
(aB kinematic plane= B2 axial
plane)

the initial folds were slip folds, although, of course, in the general case, the first fold axis β_1 would be oblique to the kinematic B_1-axis.

The solid geometry of some superposed slip folds is made more clear by Figures 302 and 303. In Figure 302 the plane of slip (the a_2B_2-plane) is perpendicular to the geometric B_1-axis of the first fold. Because the B_1-

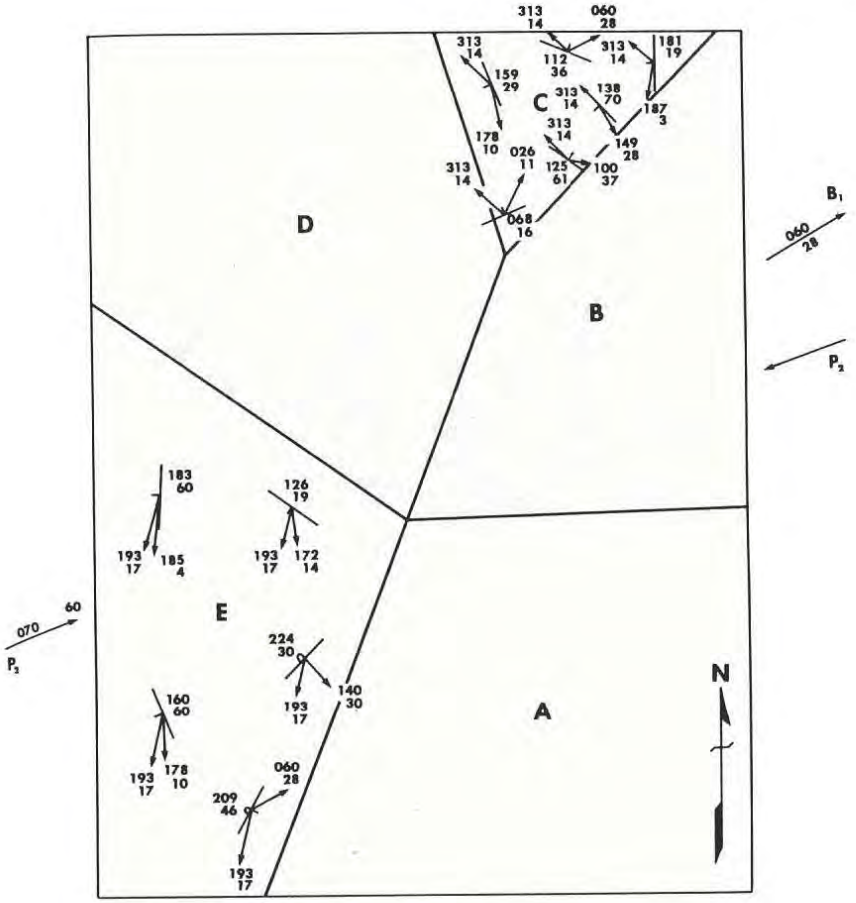

Figure 301. Schematic map of an area (Fig. 284) in which B_2-slip folding has been superposed on an initial B_1-flexural-slip fold system. See text for explanation.

axis of the synform (first fold) plunges towards the observer in Figure 303, B_1 is oblique to both c_2 and the a_2B_2-plane. With superposed slip folding the chances of the intersection of S and S' being parallel to either the a_2- or the B_2-kinematic axis are relatively small; such parallelism only tends to occur in very small volumes of rock.

As pointed out previously, the stereographic approach to folding has certain limitations because each fabric element is divorced from its actual U,V,W-location and moved to the center of the stereogram. In consequence, it is difficult to visualize the three-dimensional morphology of superposed slip folds from a stereogram. O'Driscoll (1962, 1964)

illustrated experimentally-produced patterns for some geometries that result with superposed folding, while Ramsay (1962C) described the morphology to be expected with each possible orientation of the two sets of kinematic axes.

Ramsay (1962C) demonstrated that the morphology resulting from superposed slip folds (F_1 and F_2) depends on the:

(a) morphology of the F_1-folds and the orientation of the F_1-axes,

(b) orientation of the second kinematic axes with respect to the F_1-axes; three main geometric relationships occur (see Table 2).

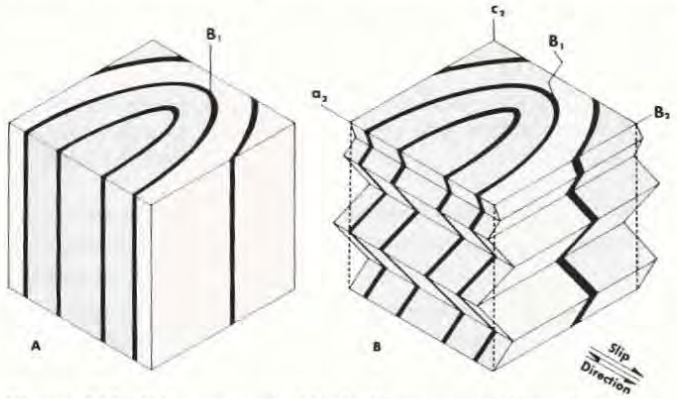

Figure 302. Diagrammatic block diagrams to show the geometry of a superposed slip fold with the plane of slip perpendicular to the first geometric fold axis. A: The first flexural-slip fold; B_1 is the geometric fold axis. B: Superposed slip fold; a_2B_2 is the plane of slip perpendicular to B_1.

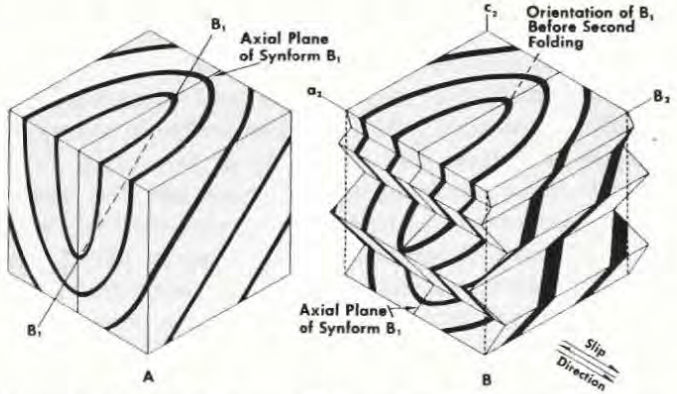

Figure 303. Block diagram to show effect of superposed slip folding, where the a_2B_2-kinematic plane is not normal to the B_1-geometric fold axis.

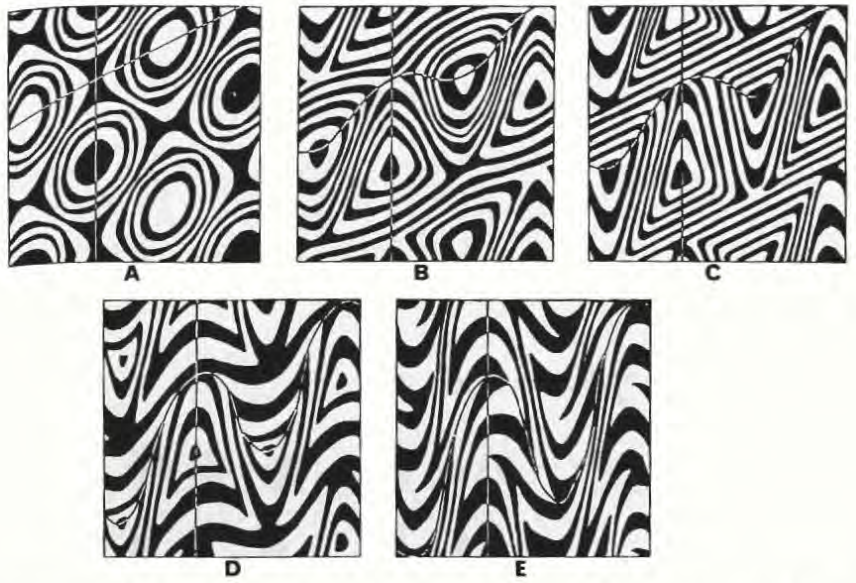

Figure 304. Main types of two-dimensional interference pattern resulting from superposed slip folding (see Table 2). Axial traces of F_1 were originally NE-SW and those of F_2 are N-S. A: Type 1 with movement direction of F_2 contained in F_1 axial plane. B: Type 1, general form. C: Type 1 with F_2 movement direction within a limb of a F_1 fold. D: Type 2. E: Type 3 (After Ramsay, 1962C, Fig. 14).

(c) intensity of F_2-folding

(d) amount of flattening accompanying F_2 (see Chapter 6), and,

(e) orientation of outcrop surface with respect to F_1 and F_2.

Of these five factors, (a) and (b) are the most critical. Ramsay (1962C,

Table 2.—Geometric Relationships Resulting From Superposed Slip Folding

Type	Angle Between a_2-Axis and Axial Plane of F_1	Angle Between B_1-Geometric Axis and Axial Plane of F_2	Illustrated in Figure Number
1	a_2-kinematic axis lies close to axial planes of F_1	Any angle	304A, 304B, 304C
2	a_2-kinematic axis highly inclined to axial planes of F_1	Medium to high angle	304D
3	a_2-kinematic axis highly inclined to axial planes of F_1	Low angle	304E

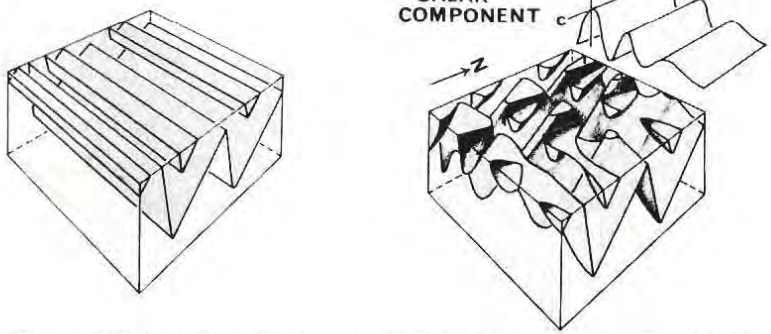

Figure 305. Interference structure resulting from superposed slip folds: Type 1 consisting of interlocking domes and basins (After Ramsay, 1962C, Figs. 1A and 1B).

p. 479) seems to have been correct in asserting that it is impossible for two sets of genuine slip folds to form simultaneously at exactly the same U,V,W-location.

The geometry of Type 1 (Table 2) is illustrated in Figure 305; domes result where antiformal axes cross and basins form where synformal axes cross. Figure 306 shows an excellent small-size example from the feldspathic sandstones (metamorphosed to the garnet grade) in the Moine Series, Loch Monar area, western Scotland; because (a) both fold sets have axial-plane foliation, and (b) the F_1-axial planes are slightly deformed and the F_2-axial planes are planar, it is reasonable to conclude that these fold sets formed separately, (i.e., not contemporaneously). Surprisingly steep domal and basinal folds result from superposed folds of this type; Ramsay reconstructed a scale model of an acute dome about 10 cm. across by cutting serial sections through a sample of banded hornblende-biotite-Lewisian gneiss from Glenelg (Fig. 307). With such geometry the change in plunge of individual folds is often greater than 90°.

Type 2 gives rise to crescentic and mushroom-shaped outcrop patterns (Fig. 308) that are commonly developed where tight recumbent folds of any size have been refolded. Ramsay illustrated an example from an outcrop 25 cm. across, in which isoclinal refolding of older isoclinal folds occurs within the Moine metasedimentary rocks at Ben Clachach, Loch Hourn area, western Scotland; folded metasedimentary rocks exposed in a 130 sq. km. map area near Marangudsi, Rhodesia, show an analogous pattern, although this example is many times the size of the Scottish example (Ramsay, 1962C).

The geometry of Type 3 (Fig. 309) is commonly developed in regions deformed during successive phases of the same orogeny, where the

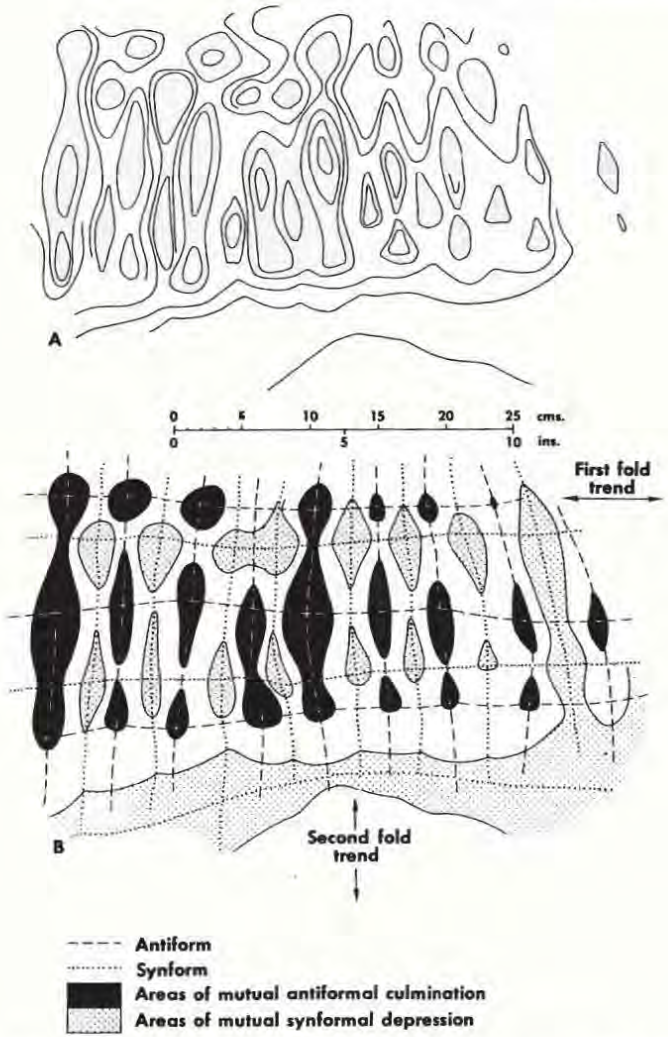

Figure 306. Closed fold forms resulting from superposed folds in feldspathic Moine sandstones, Loch Monar area, Northern Highlands, Scotland. A: Pattern of bedding planes on exposed surface. B: Analysis of domes and basins that are arranged in a regular manner along the trend lines of the two fold sets (After Ramsay, 1962C, Fig. 3).

B-geometric axes of each pulse may be parallel to subparallel (Ramsay, 1962C, p. 476). Closed outcrop patterns are not common with this geometry because B_1 lies close to the F_2-axial plane. Ramsay illustrated a small-sized example of this type of folding from the Lewisian hornblendic gneiss near Arnisdale, Loch Hourn, western Scotland.

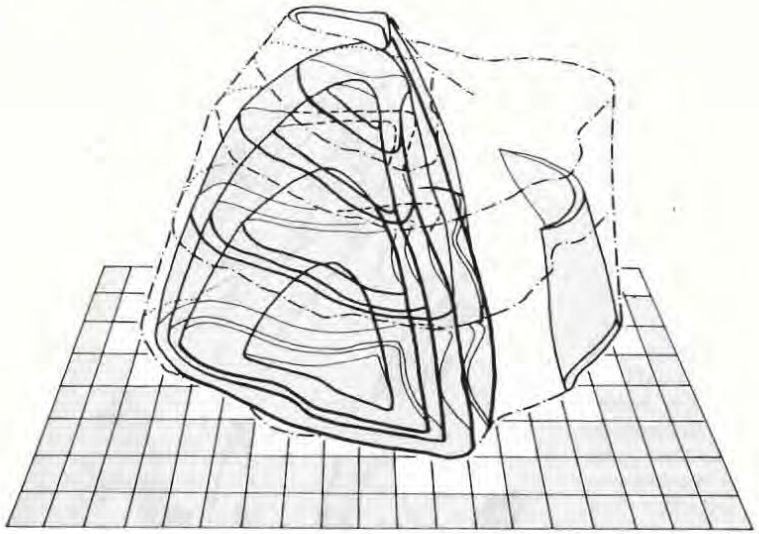

Figure 307. Diagrammatic reconstruction of an acute culmination dome in Lewisian banded hornblende-biotite gneiss, Glenelg, Northern Highlands, Scotland; the model is based on five serial sections (dot-dash lines) cut through a hand sample. Individual lithologic members are picked out by heavy solid lines; the model stands on a 1 sq. cm. grid (After Ramsay, 1962C, Fig. 6).

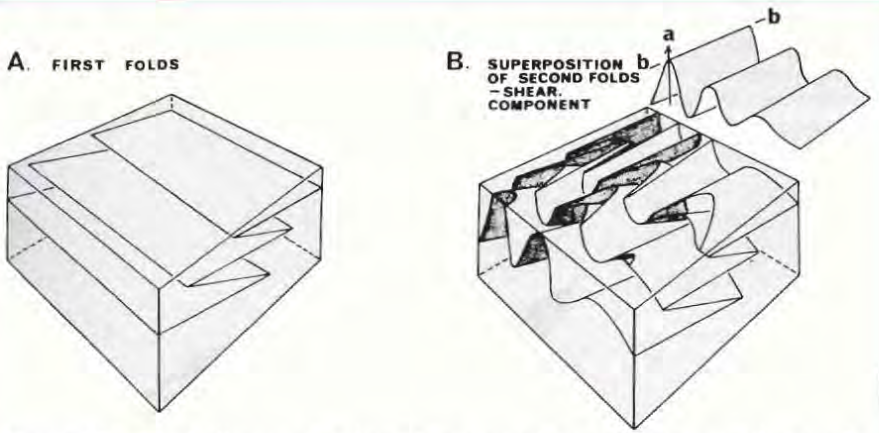

Figure 308. Block diagrams to show the crescentic outcrop patterns that result from superposed slip folding on recumbent first folds (Ramsay's Type 2). A: The first folds. B: Geometry resulting from superposed slip folds; the amount of second slip is indicated in the inset (After Ramsay, 1962C, Figs. 8A and B).

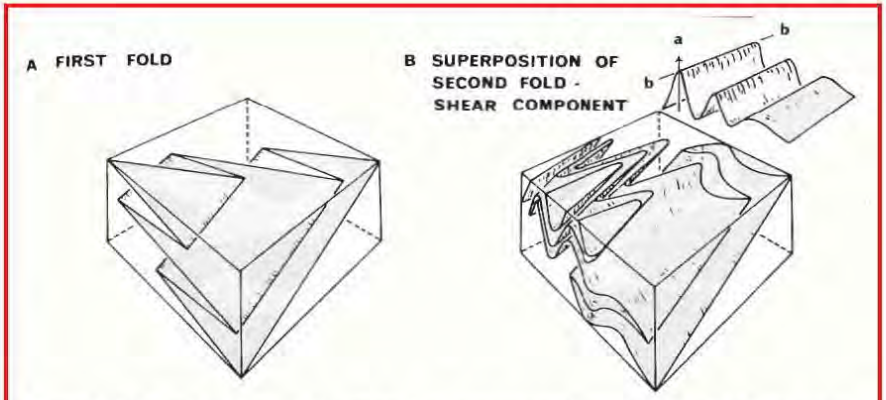

Figure 309. Block diagrams to show the outcrop patterns that result from superposed slip folding of plunging recumbent first folds (Ramsay's Type 3). A: The first folds. B: Geometry resulting from the superposed slip folds; the amount of second slip is indicated in the inset (After Ramsay, 1962C, Figs. 11A and B).

It seems likely that additional factors may also be involved in the generation of some "eyed" or circular fold patterns; for example, Nicholson (1963) found examples in the Sandvand Grey Marble, northern Norway, that are more irregular in form and areal distribution, and he invoked localized diapiric action (cf. comparable to miniature salt tectonics) superposed on a first generation of folds to explain their geometry.

When extensive continuous outcrops are exposed, an analysis of the symmetry surfaces drawn with respect to the folded oldest *S*-structure (e.g., bedding) can sometimes lead to a more direct understanding of the fold geometry (Carey, 1962A).

Relatively simple geometry results when the two superposed sets of slip folds have a common *B*-kinematic axis, but inclined *aB*-slip planes. In Figure 310A the original unfolded S_0-surfaces are shown. Figure 310B is the profile of first-phase slip folds (F_1), in which both the geometric and kinematic *B*-axes are normal to the page; the profile of an individual S_0-surface is shown in Figure 310C. Figure 310D shows the profile which would result from second-phase slip folds (F_2) affecting horizontal S_0-surfaces, such as those in Figure 310A. If slip with F_2-geometry is superposed on the F_1-folds (Fig. 310B), the complex pattern of Figure 310E results. Carey (1962A, p. 99) demonstrated that different geometric patterns develop if the kinematic patterns are reversed in time; thus, Figure 310F is the profile that results from F_2 (Fig. 310D) occurring before F_1 (Fig. 310C).

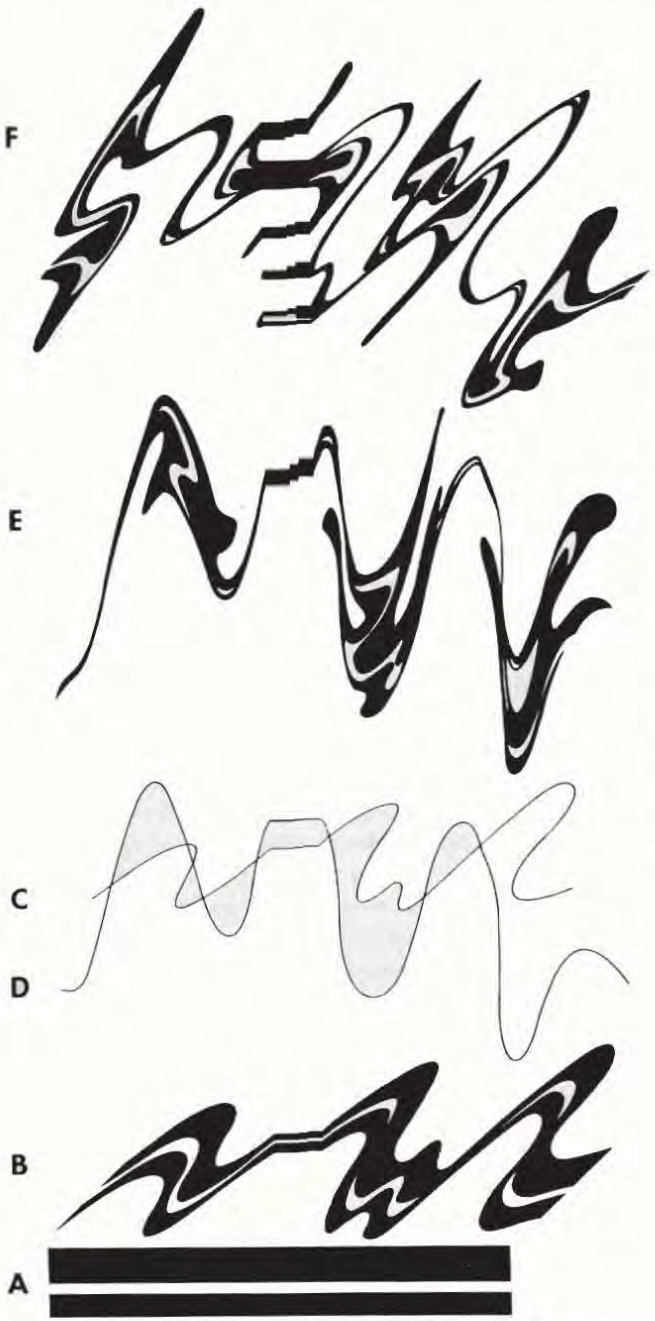

Figure 310. The geometry of superposed slip folds with common *B*-kinematic axes, but inclined *aB*-slip planes. A: Original unfolded S_0. B: Profile of F_1-slip folds. C: Profile of an individual F_1-fold. D: Profile that would result from F_2-folding of undeformed S_0. E: Profile resulting from F_2-slip folds superposed on F_1-folds. F: Profile that would result if F_1 geometry were superposed on an earlier F_2-fold system (After Carey, 1962A, Fig. 5).

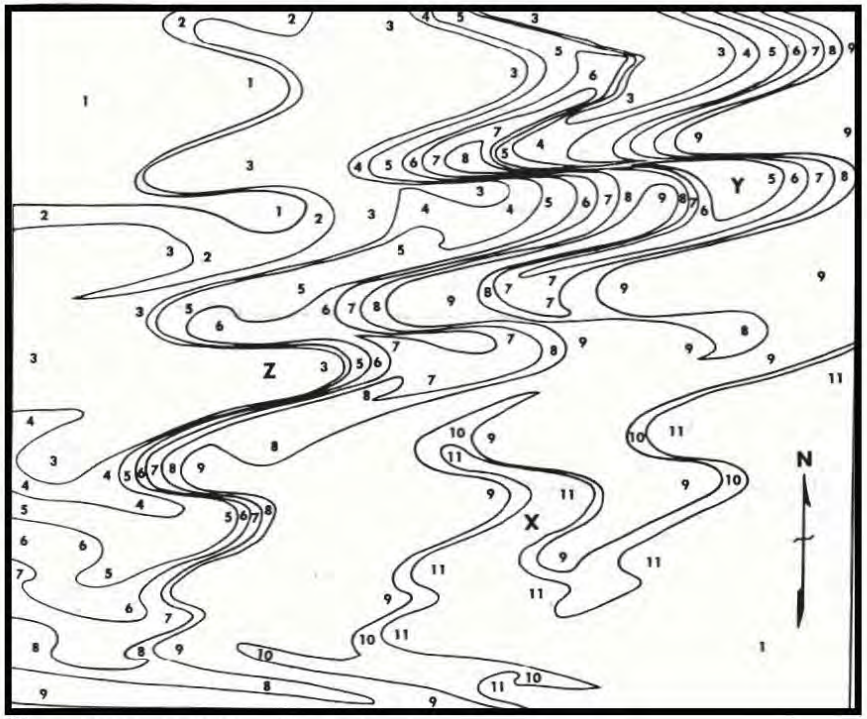

Figure 311 (top). Fold profile produced by two phases of slip folding: see text for explanation (After Carey, 1962A, Fig. 10). Figure 312 (bottom). Sequence of rocks derived from Fig. 311 (After Carey, 1962A, Fig. 11).

Carey (1962A) outlined a simple method for unravelling complex profiles like those of Figures 310E and 310F. Suppose Figure 311 is a profile with respect to two phases of folding (i.e., similar to those in Fig. 310). The successive lithologic units can now be numbered; the sequence of numbers in Figure 312 is consistent but implies relative age. Individual lithologic units may be sheared out, as at Z in Figure 312 where units 3 and 8 are almost in contact. With the aid of these numbered lithic units, symmetry axes can be traced across the map-area (Fig. 313); the symmetry referred to here is a crude numerical repetition which, for example, is shown at the point X which lies at the center of the sequence 9-10-11-10-9, and by Y that lies at the center of the sequence 9-8-7-6-5-6-7-8-9. By connecting up such symmetric points, two sets of traces can be drawn on the profile (Fig. 313), namely (a) a subparallel set of more or less straight lines and (b) a subparallel set of strongly flexed lines.

If it is assumed that both phases of deformation were dominated by slip folding, the more or less straight lines of symmetry must have been produced during the second or F_2-phase. Hence, the curved lines represent F_1-axial-plane traces refolded by F_2; if a composite tracing of these curved lines is made (Fig. 314C), the mean trace can be approximated (Fig. 314D). To remove the effects of F_2 the mean trace (Fig. 314D) is converted to a straight line by moving the structures parallel to the trace b of Figure 314. Figure 315B shows this operation completed for the original profile (Figs. 311 and 315A); unfortunately, this operation involves an arbitrary set of nonaffine slip movements because, although the line d (Fig. 314) must be made straight, it could be made perpendicular to b or any other arbitrarily-chosen angle to b. Without external evidence, which may be very difficult to find, the selection of a trace for the plane of symmetry of F_1 must remain arbitrary.

The F_1-folding can now be removed from the profile in Figure 315B. By making a composite tracing of the lithologic bands in Figure 315B, the mean fold profile is determined (Fig. 315C and 315D). The mean is transformed into a straight trace by slip movements parallel to the axial plane of F_1. As with removing the effects of F_2, the orientation of the straightened trace is purely arbitrary, unless there is some outside evidence for the original orientation. Hence, Figure 315F is only one possible interpretation of the pre-F_1 geometry.

In actual field examples the geometry is commonly more complicated to unravel, because it is unlikely that any random outcrop surface will contain the *a*-kinematic axis for both the F_1 and F_2 folds. In the examples described above, the *a*-kinematic axes are always in the plane of the paper. If *a* is oblique to the exposed outcrop surface for either or both phases of folding, an additional element of distortion is introduced.

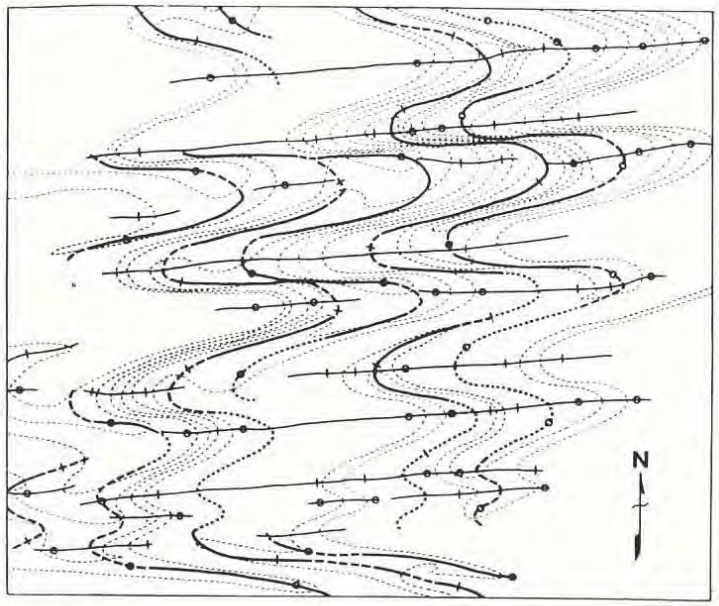

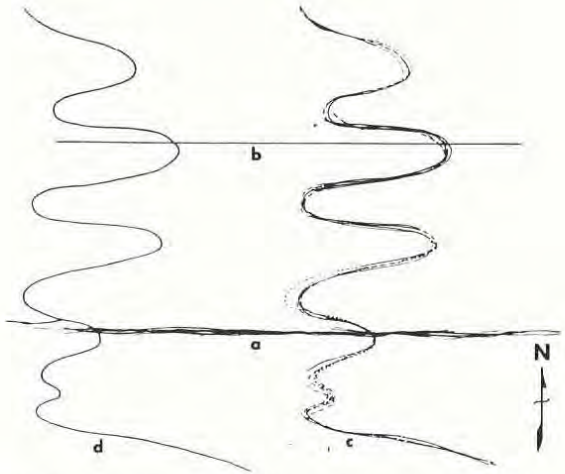

Figure 313 (top). Symmetry axes (fold axes) derived from Figure 312. The original bedding (light dotted lines) is receding and the involuted axial surfaces of the first folds, which act as *S*-surfaces for defining the second folds, become more prominent (After Carey, 1962A, Fig. 12).

Figure 314 (bottom). Determination of the mean directrix and mean fold profile of superposed folds recorded in Figure 313 (After Carey, 1962A, Fig. 13).

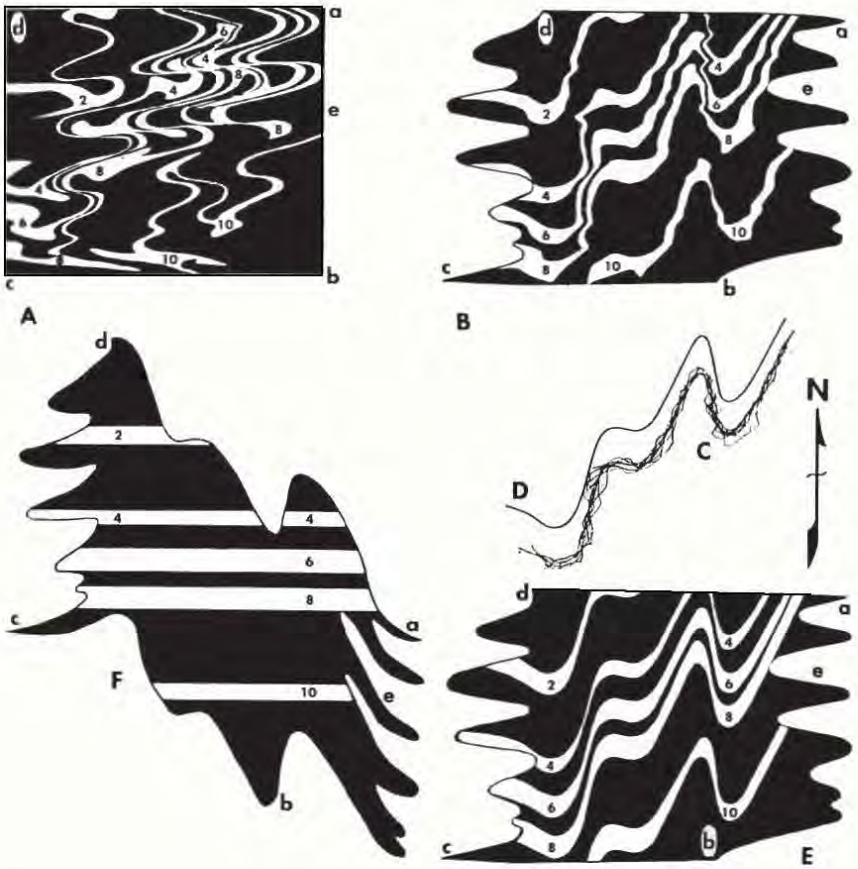

Figure 315. Resolution of superposed slip folds to the original beds. A: Final profile resulting from F_2 superposed on F_1-slip folds. B: Initial removal of F_2-folding. C: Successive bed profiles superposed from B. D: Mean fold profile from C. E: Profiles from B smoothed by use of the mean profile in D. F: Removal of D from profile in E to reproduce the original strata. a, b, c, and d mark the positions assumed by the original corners of A (After Carey, 1962A, Fig. 14).

These constructions suggested by Carey (1962A) provide considerable insight into the geometry of superposed slip folds, but their practical application is limited because of the required restraints on the geometrical relationships between F_1 and F_2. As shown above, many other geometric relationships commonly occur.

Ramsay (1962A, 1962C) suggested that "flattening" is an important factor in slip folding (see Chapter 6); if flattening effects are superposed on the F_2-slip folds, the geometry of both the F_1 and the F_2 structures will be distorted, and thus be more complex.

CONCLUDING REMARKS

As in the case of folding limited to a single phase, in superposed folds each period of deformation can incorporate elements of both flexural-slip and slip folding; interplay of the two types naturally complicates the geometric pattern developed.

After an area has been penetratively folded, it is possible for the same area to develop new folds at a subsequent period with an amplitude several times larger than the first folds. In terms of the regional gross stratigraphic units, such second folds can be cylindroidal, although, with respect to individual *S*-surfaces folded during the first phase, the superposed folds would tend to develop conical structures. Hence, when starting to investigate a new area, it is important to determine the size of the domains within which structures are cylindroidal. When structures associated with two periods of folding are both visible in exposures of the same size, it is a general rule that, where the largest folds are cylindroidal, the F_2-folds are always smaller than the F_1-folds, because they (F_2) can only form on the planar limbs of the F_1-folds (Weiss, 1959B, p. 98). This rule applies to both superposed flexural-slip and slip folds. In studies of progressive metamorphism and deformation, successive flexures have smaller amplitudes (see Chapter 11); however, very early structures are often small in size, but are obliterated by later, thoroughly penetrative deformations; folding episodes subsequent to such penetrative deformations commonly tend to be of smaller and smaller sizes.